# Synthesis, structure characterization and study of a new kind of catalyst

Hasan, Ahmad; Essa, Khamis; Gomaa, Mohamed

*DOI:*
10.3390/en15207575



*Document Version*
Publisher's PDF, also known as Version of record

*Citation for published version (Harvard):*
Hasan, A, Essa, K & Gomaa, M 2022, 'Synthesis, structure characterization and study of a new kind of catalyst: a monolith of nickel made by additive manufacturing coated with platinum', *Energies*, vol. 15, no. 20, 7575. https://doi.org/10.3390/en15207575

*energies*

MDPI

*Article*

# Synthesis, Structure Characterization and Study of a New Kind of Catalyst: A Monolith of Nickel Made by Additive Manufacturing Coated with Platinum

**Ahmad O. Hasan [1,2], Khamis Essa [2] and Mohamed R. Gomaa [1,*]**

[1] Department of Mechanical Engineering, Faculty of Engineering, Al-Hussein Bin Talal University, Ma'an 71110, Jordan
[2] School of Mechanical Engineering, University of Birmingham, Birmingham B15 2TT, UK
* Correspondence: behiri@bhit.bu.edu.eg

**Abstract:** The monitoring of environmental contamination is an important issue to protect human health and the atmospheric environment. In this study, the optical imaging of mesh structures not coated and coated with platinum was performed to analyze the optical characteristics of the lattices. A nickel monolith catalyst was manufactured via additive manufacturing and coated with platinum, and it was presented to characterize the catalyst properties. The analysis focused on the process of coating using hydrazine bath as a reducing agent. The results showed an increase in the thickness of the coating with baths with durations of 1.5 h, 2.0 h and 2.5 h. The coating thickness was strongly dependent on time duration. The SEM images and EDX were used to confirm the process of coating and analyze the presence of platinum on the catalyst. Coating layers were very thin, and others were not homogeneous over the surface. When the catalyst was exposed to platinum for 2.5 h, the catalyst showed an efficiency of 0.06% for NOx, 0.10%, for CO and 0.09% for HC reduction.

**Keywords:** nickel; platinum catalyst; platinum coating; SEM and EDX images analyses; NOx; CO; HC emissions; compression ignition engine



**Citation:** Hasan, A.O.; Essa, K.; Gomaa, M.R. Synthesis, Structure Characterization and Study of a New Kind of Catalyst: A Monolith of Nickel Made by Additive Manufacturing Coated with Platinum. *Energies* **2022**, *15*, 7575. https://doi.org/10.3390/en15207575

Academic Editors: Haifeng Liu and Zongyu Yue

Received: 23 August 2022
Accepted: 10 October 2022
Published: 14 October 2022



## 1. Introduction

The complex reactions that take place during fuel combustion are not yet fully understood [1,2]. The air/fuel (A/F) ratio is considered to be one of the main sources of HC emissions formation during combustion [3–7]. Furthermore, spark ignition (SI) and combustion such as gasoline direct injection (GDI), which are able to operate with stoichiometric or lean and rich mixture conditions, make operation for catalysts and emissions conversion difficult, meaning controlling the combustion pollutants becomes challenging. Treatment management to control exhaust emissions has been taking place for almost four decades, with hard work in the automotive industry to overcome the difficulties of controlling exhaust emissions and create highly effective technologies. However, there are still some challenges facing researchers, such as low-temperature engine combustion, which releases high amounts of unburned hydrocarbon. By the 1980s, the Three Way-Convertor (TWC) was presented to control NOx, CO and HC simultaneously [8]. However, the selection of catalysts supports for the synthesis of heterogeneous catalyst matters has been investigated earlier, such as aluminum oxide ($Al_2O_3$), calcium oxide, (CaO), magnesium oxide (MgO), etc., due to their high stability and porosity [9–12].

Despite the evolution of cleaner fuels and combustion technologies, diesel combustion engines release plenty of nitrogen oxides (NOx), particulate matter (PM) and soot particles compared to SI engine emissions. The solution to decrease NOx and PM emissions is using i: exhaust gas recirculation (EGR); ii: and selective catalytic reduction (SCR); iii: diesel particulate filters (DPFs); in addition, more options are available for diesel combustion such as alternative fuels such as biofuels and gas to liquid (GTL) fuels. Gases emitted from

modern diesel engines still require a modern advanced after-treatment system to meet the required emission legislation [13–18]. Diesel engines have high performance, good fuel economy, durability, high torque capability and no throttling losses. Diesel vehicles release particulate matter which consists of different types of chemical components such as organic carbon, trace elements, elemental carbon, inorganic ions, etc. It is highly harmful to humans and the environment, as they cause severe respiration problems. Conditions of excess oxygen (HC-SCR) have received much attention as one of the most promising and straightforward methods for reducing NOx emissions. Extensive research has been undertaken using different types of hydrocarbons as reductants [19–23]. However, although a number of catalysts have been tested in the HC-SCR, no catalyst has been considered suitable for the diesel de-NOx conditions. In these conditions, the catalysts are required to be hydrothermally stable and active at relatively low temperatures in the presence of sulfur oxides (Sox) and water vapor. Many base oxides/metals (e.g., $Al_2O_3$, $TiO_2$, $ZrO_2$ and MgO with these oxides promoted by, Pt, Co, Ni, Cu, Fe, Sn, Ga, In and Ag compounds) are active catalysts for HC-SCR of NOx [24,25].

NOx reduction activity occurs at a narrow temperature window of 200–300 °C, which is also associated with the formation of $N_2O$. Moreover, zeolite-based catalysts, which are the majority of the de-NOx catalysts reported in the literature, are unlikely to be suitable as automotive catalysts due to their instability under hydrothermal conditions [26–28].

Variations in catalyst dosage, irradiation period, solution pH, and phenol content were used to investigate photo catalytic degradation. The results showed that, at pH 5, with 20 mg of $TiO_2$ NPs photo catalyst and 10 mg/L phenol in water, composite nanofibers had the highest activity; this high activity is due to the presence of more active binding sites exposed on the surface of $TiO_2$ NPs cross-linked on the nanofibers' surface, as well as the separation of electron–hole pairs being more effective.

The use of photo catalytic composite nanofiber membranes to degrade malachite green and acid red 27 to non-toxic and innocuous compounds was investigated. Electro spinning was used to make the PAN/$SiO_2$-$TiO_2$-$NH_2$ nanofiber membrane, which was then chemically cross linked, and the effective fabrication of a nanofiber membrane was validated using scanning electron microscope (SEM), energy dispersive X-ray (EDX), Fourier transform infrared (FTIR), and X-ray diffraction (XRD) findings.

The results demonstrate that, with an excellent distribution of $SiO_2$ and $TiO_2$ on the PAN nanofiber membrane surface, the PAN/$SiO_2$-$TiO_2$-$NH_2$ nanofiber membrane exhibited the maximum deterioration, and with artificial visible light (125 W irradiation), the 100% photo degradation of MG and AR 27 was obtained after 9 and 25 min, respectively. Furthermore, the nanofiber membrane displayed high photo degradation stability and reusability for MG and AR 27 and had the potential to be used in industrial applications. In [29,30], these studies showed that the porous coordination polymers of Mg (II) dihyroxyterephtalate (Mg-MOF-74) were synthesized, characterized and evaluated for the catalytic cyclo addition process between carbon dioxide $CO_2$ and propylene oxide at varied Ptx loadings to create propylene carbonate; the reaction was examined at temperatures ranging from 100 °C to 170 °C and pressures ranging from 9.1 bar to 19.5 bar, as well as reaction durations ranging from 4 h to 15 h. In the presence of dimethyl formamide (DMF) and dichloromethane (DCM), which serve as solvents and promoters for the reaction, the results reveal that increasing Pt loading on the catalyst surface enhances selectivity toward propylene carbonate, and the number of uncoordinated MgO sites in the Mg-MOF-74 framework structure grows. The number of uncoordinated MgO defect sites and PO conversion both increased progressively with Pt loading and PC selectivity during the reaction. When Ptx/Mg-MOF-74, DMF, and DCM are used together, they have a synergistic impact that outperforms using them separately.

Trash disposal which produced suitable biomass from date pits was explored for use in the manufacturing of green carbon catalysts and biodiesel. The Taguchi technique of Response Surface Methodology (RSM) was used to investigate the influence of many process factors on the yield of biodiesel generated, including the reaction temperature, time,

catalyst type, and methanol to oil ratio. When the process temperature was set to 65 °C, the catalyst type C3 (6 percent KOH on carbon) was used and the methanol to oil ratio was set to 9:1, the optimal yield was 91.6 percent [31,32].

More studies have attempted to understand the combustions and emission characteristics of spark ignition engines fueled by gasoline, methane, ethane, propane and hydrogen; when using pure ethanol and methanol instead of gasoline, the power of the engine decreased and tailpipe emissions such as CO and NOx were reduced, while fuel consumption was increased [33,34]. Another study found that the toxicity of exhaust gases decreased with an increase in engine load. The average concentration of total-PAHs emitted using biofuel with percentages of B25 and B50 fuels were from 11.7% to 54.8% lower than those from B0 at all engine loads. Additionally, the concentration of aliphatic emissions was negligible compared to aromatic compounds [35,36]

The aim of this study was to build a new catalyst with a nickel monolith, manufactured via additive manufacturing and coated by platinum, which had very good chemical and physical properties (good resistance to corrosion and stable at a high temperature), and as a catalyst, black powder was used to catalyze a reaction at a high temperature. A coating process was carried out under different time durations, and catalytic tests were carried out under different engine conditions to observe the catalyst efficiency of eliminating HC, CO, $CO_2$ and NOx emissions.

## 2. Methodology

### *2.1. Design and Selective Laser Melting Additive Manufacturing of the Specimens*

The selective laser melting additive manufacturing process is used to fabricate three-dimensional (3D) structures by adding layer upon layer at a time. According to the material chosen for the object, selective laser melting (SLM) was used. The lattice was melted and fused into powder layers on top of each other according to the designed model. The method required an absolutely inert atmosphere to avoid pollution, and the design was based on diamond unit cells, as shown in Figure 1. The strut diameter was set to 400 µm, and the strut length was 2 mm. The lattice was designed to have dimensions of 20 × 20 × 11 $mm^3$.

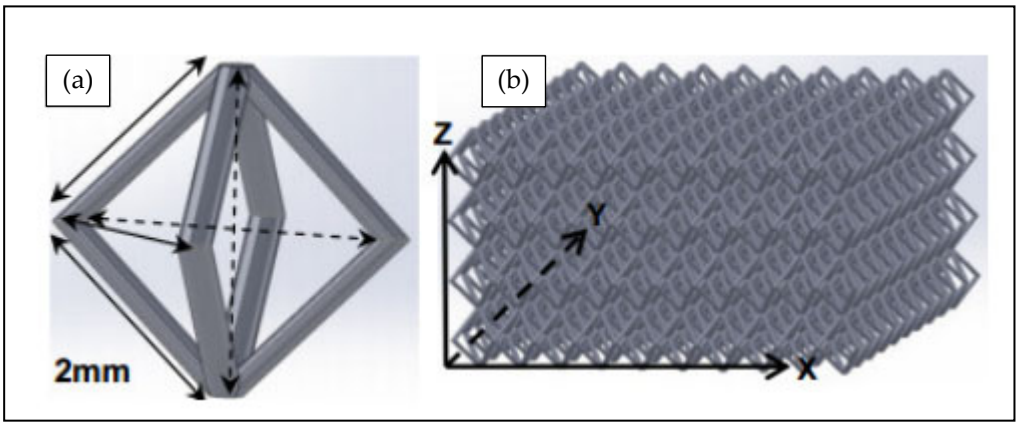


**Figure 1.** (**a**) CAD model of a diamond unit cell and (**b**) CAD model of lattice structure for SLM building.

### *2.2. Electro Less Deposition of Platinum*

Platinum coating is the process of nickel coating with platinum using a hydrazine bath as a reducing agent.

The experiment was carried out according to the European patent EP0423005A1 [37]. The bath contained three key compounds: a platinum compound ($H_2Pt(OH)_6$), a reducing agent ($N_2H_4$, $H_2O$) and a stabilizing agent ($As_2O_5$). The compounds were prepared in two stages: i: a stock solution of platinum was prepared as shown in Figure 2. ii: the bath was reduced and stabilized. The platinum hydroxide was not stable enough to ensure stability

towards the reducing agent; it had to form a complex with oxidation. For that, the next steps were followed:

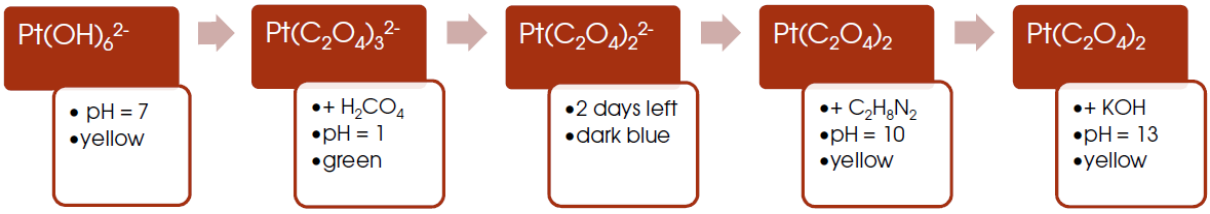


**Figure 2.** Preparation steps of the hydrazine bath.

Table 1 presents the average thickness of the coating according to the duration in the electro less bath. After being rinsed with deionized water and washed with ultrasonic cleaner, the samples were prepared for deposition in the bath, and after being deposed for a few minutes, the bath became darker and it was difficult to see the samples.

**Table 1.** Average size of coating with time duration.

| Duration of Deposition | Thickness of the Coating |
|---|---|
| 1.5 h | 0.73 µm |
| 2.0 h | 2.66 µm |
| 2.5 h | 4.43 µm |

After one hour, hydrazine was added to reload the bath.

### *2.3. Catalyst Characterization*

SEM was used to estimate the homogeneity and thickness of the sample coating, and three images were taken on each sample on different magnifications with different time durations of 1.5 h, 2.0 h and 2.5 h. The presences of element components of the final catalysts were detected using energy dispersive X-ray spectroscopy (EDX).

## 3. Experimental Setup

### *3.1. Engine*

The new catalyst efficiency was tested using a Lister Peter TR1, naturally aspirated, air-cooled, single-cylinder, direct injection engine (Figure 3). Standard commercial diesel fuel was used in this test under different engine conditions (Table 2). The injection timing was kept at 22° CA before top dead center (bTDC) according to manufacturing specifications. An adjustable valve was installed in the tailpipe in order to obtain a portion of the exhaust. The engine exhaust gas was controlled by an adjustable valve and fed to the mini-reactor through a heated flexible steel pipe kept at 200 °C with a heater line to avoid hydrocarbon condensation.

**Table 2.** Engine conditions.

| Exhaust Flow Rate | Engine Speed (rpm) | Exhaust Temperature (°C) | Oxygen (%) | Engine Load | GHSV ($kh^{-1}$) |
|---|---|---|---|---|---|
| 1 L/min | 1500 | 380 | 0.02 | 8 Nm | 25 |
| 1 L/min | 2000 | 360 | 0.01 | 8 Nm | 27 |
| 1 L/min | 2500 | 345 | 0.01 | 8 Nm | 24 |

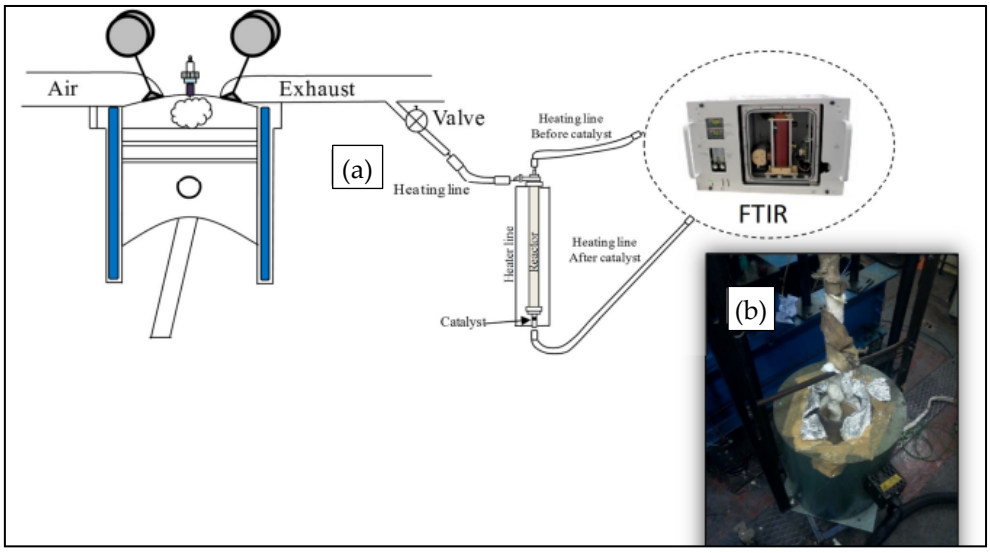


**Figure 3.** Schematic experimental set up (**a**) and the real reactor (**b**).

### *3.2. Emission Analyzer*

The catalyst was fitted inside the reactor to be fed with exhaust gases. Fourier Transform Infrared Spectroscopy (FTIR) 2100 MKS (Figure 4) was used to measure the sample which was earlier pumped via a heated line maintained at 190 °C. The catalyst was placed after the exhaust, tightened from both sides to the exhaust pipes and connected via a heating line to the emission analyzer (FTIR).

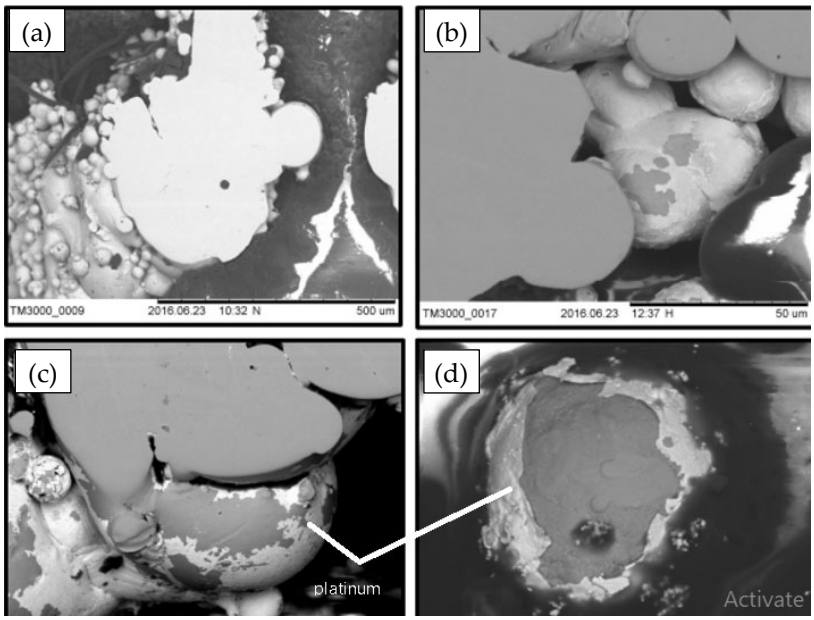


**Figure 4.** SEM images of the sample without coating (**a**) MAG 200×, coated during 1.5 h; (**b**) MAG 1500×, coated during 2.0 h; (**c**) MAG 600× and during 2.5 h; (**d**) MAG 2500×.

### *3.3. Measurements*

All measurements had uncertainty, as seen in Table 3.

**Table 3.** Uncertainty.

| S.N | Parameter Name | Instrument Uncertainty |
|---|---|---|
| **1** | Load (Nm) | ±0.01 |
| **2** | Temperature | ±1 °C |
| **3** | Speed (rpm) | ±10 |
| **4** | CO (ppm)) | ±0.01 |
| **5** | HC (ppm) | ±0.01 |
| **6** | NOx (ppm) | ±0.01 |
| **7** | $CO_2$ (%) | ±0.01 |
| **8** | $H_2O$ (%) | ±0.01 |
| **9** | $H_2O$ condensation | ±0.01 |
| **10** | Thickness of coating (µm) | ±0.01 |
| **11** | Crank angel degree (° CA) | ±0.1 |

## 4. Results and Discussion

### *4.1. Catalyst Characterization*

The brightest surface in Figure 4 represents the platinum coating. As seen in the figures, the coating is not homogeneous, and some areas of the nickel specimen are not coated (dark grey). The average thickness was calculated by analyzing different areas in the obtained SEM images, and SEM images of the sample are the parameters of the quality and coating thickness (Table A1 (Appendix A)).

The EDX spectra on the sample without coating (a), coated for 1.5 h (b), coated for 2.0 h (c) and (d) coated for 2.5 h is shown in Figure 5. In each spectrum, there was platinum, nickel, chromium and cobalt; these impurities may have been due to the SLM chamber gases that might have contaminated the sample. The composition and the elementary proportions are given in Appendix A.

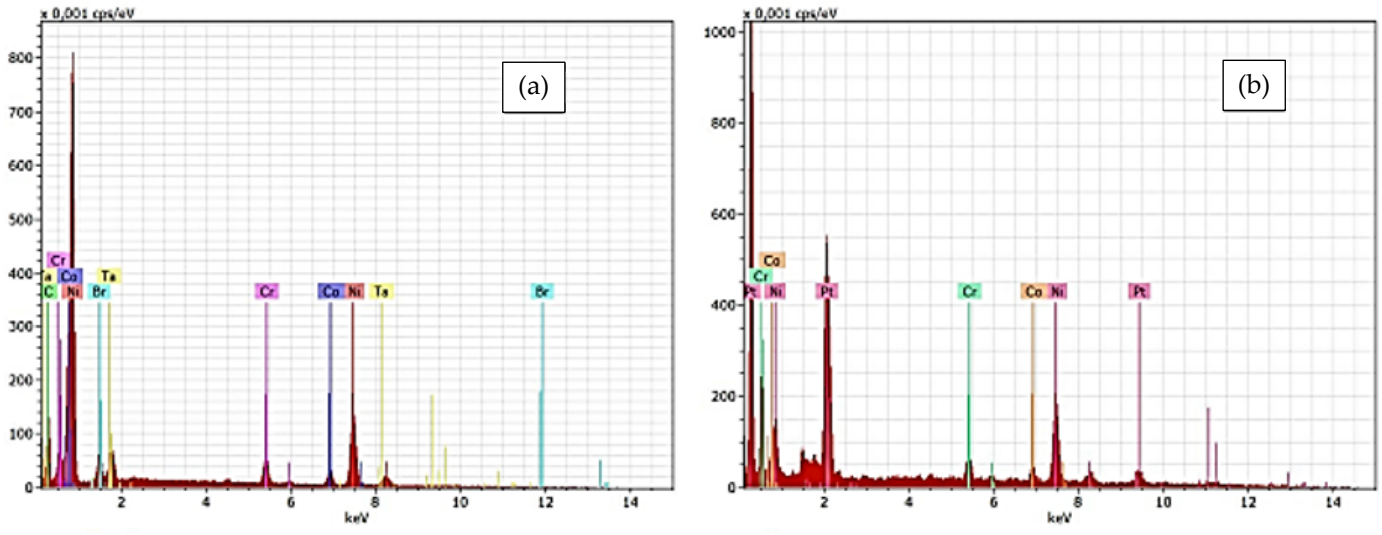


**Figure 5.** *Cont.*

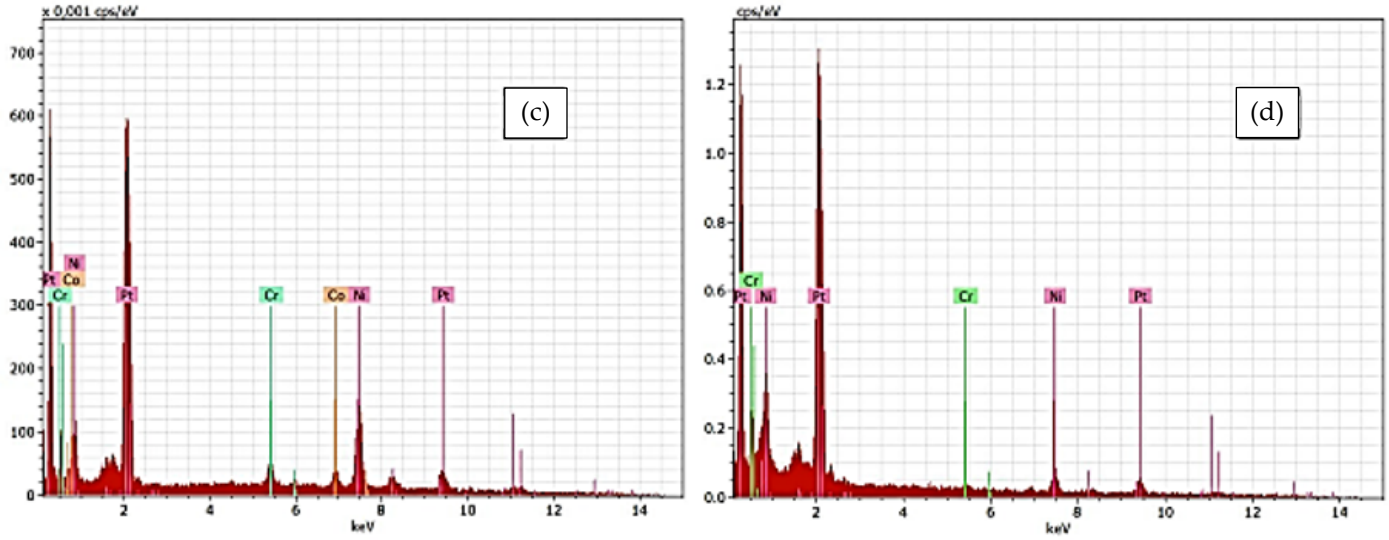


**Figure 5.** EDX spectrum on the sample without coating (**a**), coated for 1.5 h (**b**), coated for 2.0 h (**c**) and (**d**) coated for 2.5 h.

### *4.2. Catalyst Exposed for 2.0 h to Platinum*

The results presented in Figure 6 show that there was not any significant difference in gaseous emissions. The water reduced slightly, and $CO_2$ seemed to be reduced by a small percentage. In terms of regulated gaseous emissions, NOx and CO were quite similar, and high hydrocarbons were slightly reduced.

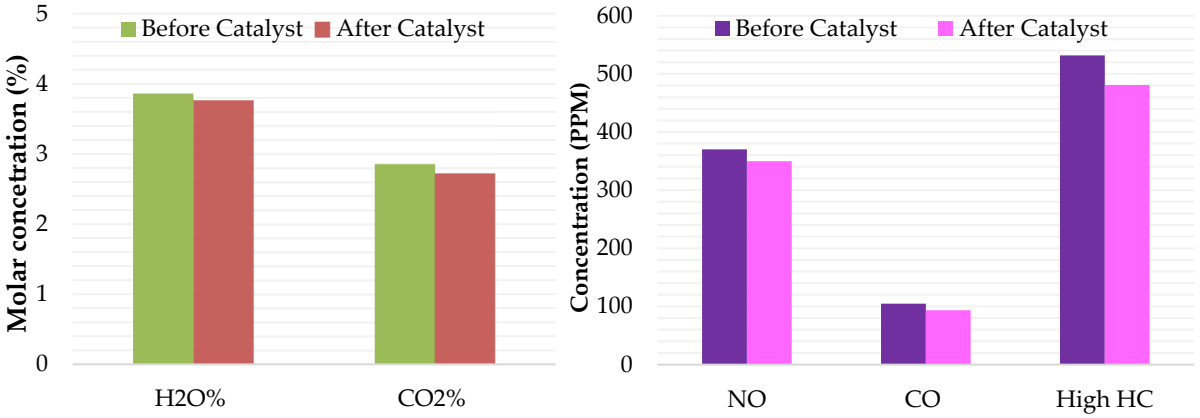


**Figure 6.** Gaseous emissions for catalyst exposed for 2 h to platinum.

In this case, the possible decrease in HC and CO achieved after catalysis is thought to be due to the space velocity of the new catalyst, since the HC and CO elimination imply an oxidation, which would produce higher concentrations of $H_2O$ and $CO_2$. The NOx reduction was around 10 ppm, which is attributed to the fact that NOx reacted with the presence of hydrocarbon in the line due to the combination of hydrocarbon and high temperature. The reduction in hydrocarbons can be due to different circumstances. The reasons could be either that part of the hydrocarbon condensates along the reactor, leading to a decrease, or hydrocarbons could react with NOx presence in the exhaust.

### *4.3. Catalyst Exposed for 2.5 h to Platinum*

The second test was carried out with a catalyst which was exposed for 2.5 h to platinum; the results showed there was not a significant effect on the emissions (Figure 7). Moreover, it was highlighted that the results changed due the precision of the equipment rather than

experiment variables. The $H_2O$ increased slightly after the catalysis; on the other hand, $CO_2$ reduced slightly and kept the same tendency that was in the previous experiment.

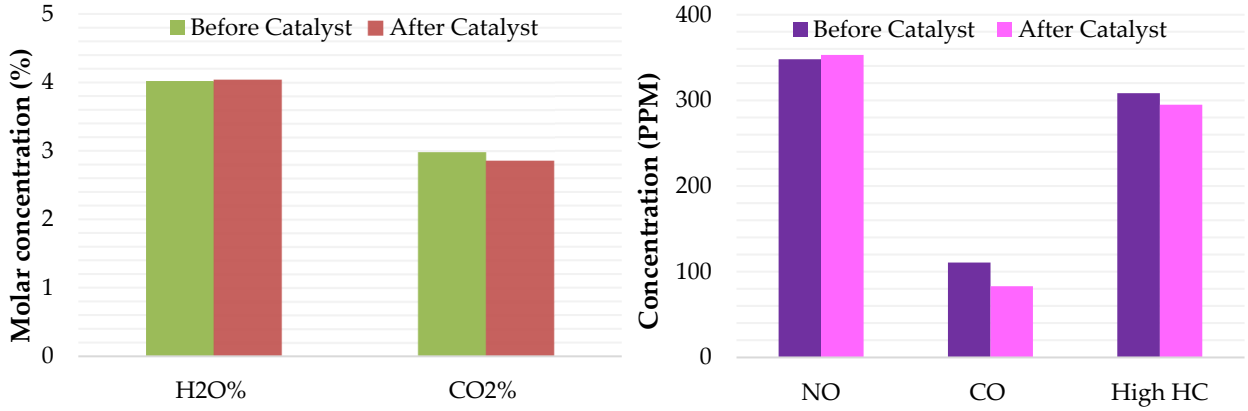


**Figure 7.** Gaseous emissions for catalyst exposed for 2.5 h to platinum.

In terms of NOx, the experiment resulted in a slight increase in NOx, which is attributed to the variability of the equipment; the hydrocarbons did not show any relevant difference between before and after catalysis. Nevertheless, the second experiment showed a general reduction of 200 ppm of HC with respect to the previous test. This effect was attributed to a higher level of the hydrocarbon condensations along the lines.

Finally, CO reported a decrease of about 30 ppm. This could be due to an oxidation in the catalyst, but we considered that it was unlikely since no increase in $CO_2$ concentration was reported after the catalysis.

According to the results, the catalyst did not show a significant emissions reduction performance; the catalyst exposed for 1.5 h to platinum was not tested as the coated catalysts, which did not show any acceptable coating quality. Flow has an important influence on the catalyst performance, and due to the limited size of the manufactured catalyst, a trade-off between the flow necessary for these catalysts and the minimum flow to feed the equipment could not be found. The minimum achievable flow rate in this experiment was not sufficient to provide any significant insight into the catalytic activity of the novel platinum–nickel catalysts.

## 5. Conclusions

The results of this study, presented the following key findings:

1- Coating process
   - i- The platinum hydroxide showed a poor stability towards the reducing agent (hydrazine bath). It must form a complex with oxalate ion.
   - ii- SEM images were used to estimate the homogeneity of the catalyst coating, and then a treatment with Image was used to measure the thickness of the layer. Analyzing the sample spectrum, simplify recognizing the composition of the surface and quantifying the proportion of each coating element.
   - iii- Coating duration has a great impact on samples' thicknesses.

2- Engine emissions
   - i- The catalyst showed a weak performance in terms of eliminating HC, CO and NOx emissions.
   - ii- Prototype catalyst efficiency could be affected by the poor homogeneity of the coated material.
   - iii- The thickness of the coated material influenced the catalyst performance.
   - iv- A comparison between the coated catalyst and an uncoated one could be conducted in future work.

**Author Contributions:** Conceptualization, A.O.H. and M.R.G.; methodology, K.E.; validation, A.O.H., M.R.G. and K.E.; formal analysis, A.O.H.; investigation, K.E.; resources, M.R.G.; data curation, A.O.H.; writing—original draft preparation, A.O.H., K.E. and M.R.G.; writing—review and editing, A.O.H. and K.E.; visualization, M.R.G. and K.E.; supervision, A.O.H.; project administration, M.R.G.; funding acquisition, A.O.H. All authors have read and agreed to the published version of the manuscript.

**Funding:** This research received no external funding.

**Data Availability Statement:** Not applicable.

**Conflicts of Interest:** The authors declare no conflict of interest.

## Appendix A

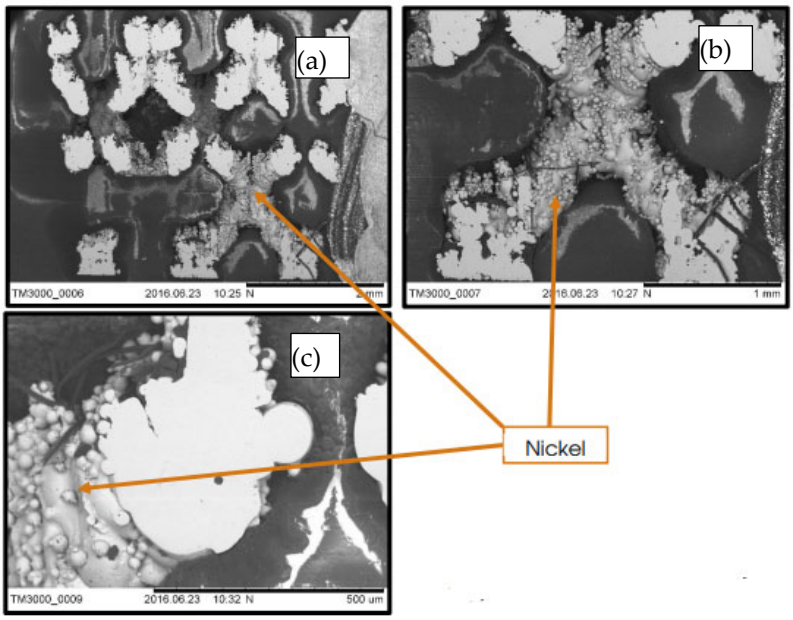


**Figure A1.** Sample without coating at magnification of 30× (**a**), 60× (**b**) and 200× (**c**).

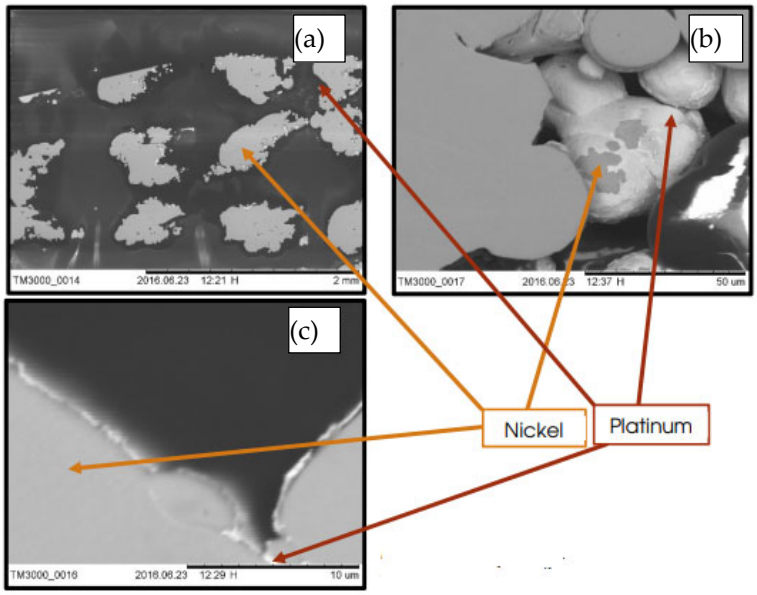


**Figure A2.** Sample coated for 1.5 h at magnification of 50× (**a**), 1500× (**b**) and 8000× (**c**).

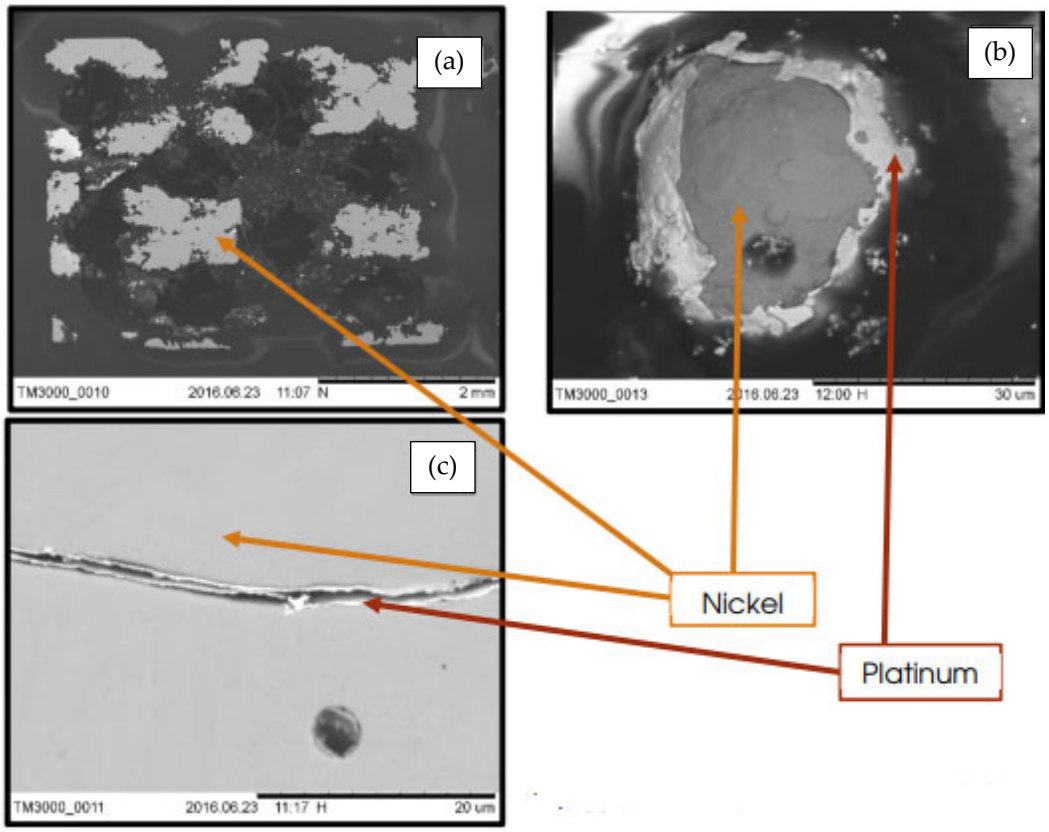


**Figure A3.** Sample coated for 2.5 h at magnification of 30× (**a**), 2500× (**b**) and 4000× (**c**).

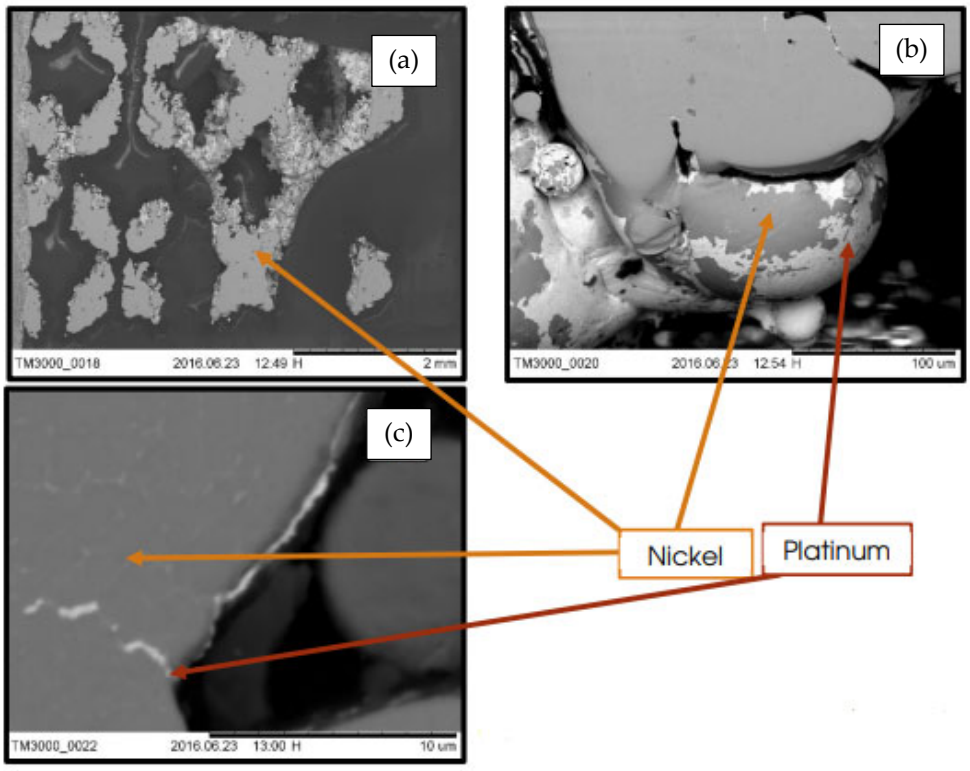


**Figure A4.** Sample coated for 2.0 h at magnification of 30× (**a**), 600× (**b**) and 9000× (**c**).

**Table A1.** Catalyst coating duration.

| Duration of Deposition | | | | | |
|---|---|---|---|---|---|
| **1.5 h** | | **2.0 h** | | **2.5 h** | |
| **Measure ImageJ** | **Thickness (µm)** | **Measure ImageJ** | **Thickness (µm)** | **Measure ImageJ** | **Thickness (µm)** |
| 138.667 | 20 | 66.002 | 10 | 61 | 20 |
| 2 | 0.655738 | 9.394 | 3.08 | 13.509 | 4.42918 |
| 2.007 | 0.658033 | 6.364 | 2.086557 | 11.667 | 3.825246 |
| 2.713 | 0.889508 | 7.826 | 2.565902 | 17.67 | 5.793443 |
| 4.197 | 1.376066 | 10.259 | 3.363607 | 16.014 | 5.250492 |
| 2.5 | 0.819672 | 6.708 | 2.199344 | 8.673 | 2.843607 |
| Average Thickness | 0.73317 µm | Average Thickness | 2.65908 µm | Average Thickness | 4.42839 µm |

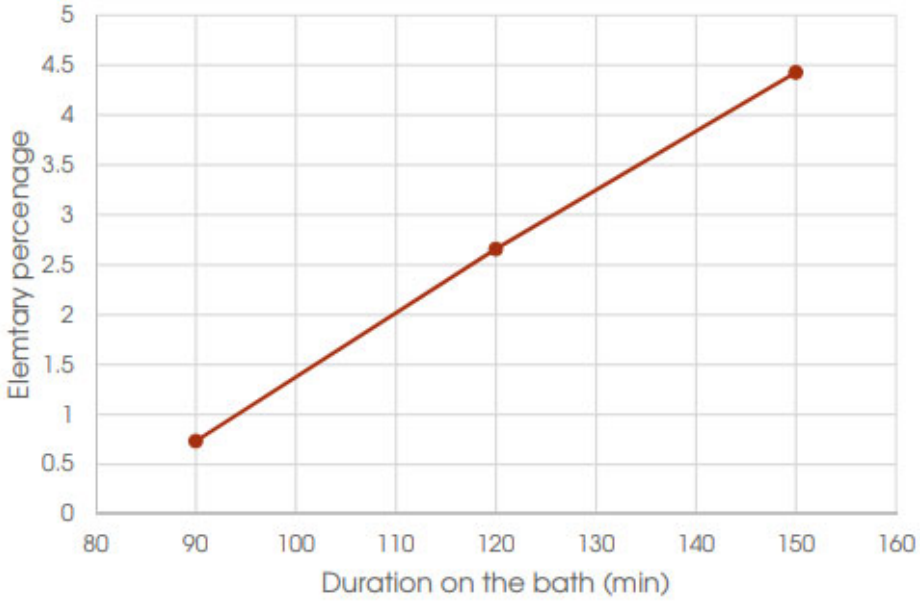


**Figure A5.** Evolution of the coated thickness according to the duration on the bath.

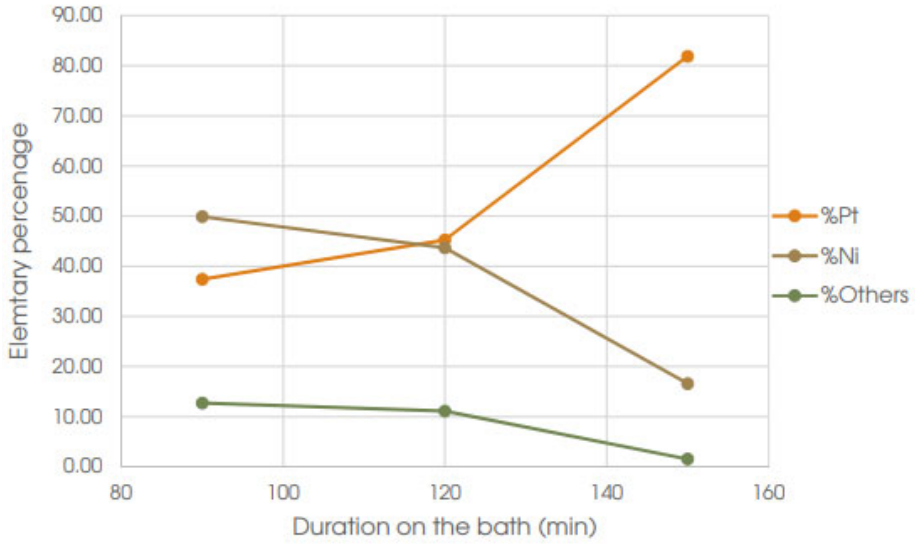


**Figure A6.** Evolution of the composition according to the duration on the bath.

**Table A2.** Results of the EDX analysis for the samples coated for 1.5 h, 2.0 h and 2.5 h.

| **During 1.5 h** | | | | | | | |
|---|---|---|---|---|---|---|---|
| **Element** | **AN** | **Series** | **Net** | **(wt.%)** | **(Norm. wt.%)** | **(Norm. at. %)** | **Error in wt.% (1 Segma)** |
| Platinum | 78 | M-series | 7978 | 37.4013 | 37.4013 | 15.0948 | 1.1637 |
| Nickel | 28 | K-series | 3051 | 49.8844 | 49.8844 | 66.9161 | 1.2724 |
| Cobalt | 27 | K-series | 539 | 7.0859 | 7.0859 | 9.4665 | 0.2023 |
| Chromium | 24 | K-series | 814 | 5.6283 | 5.6283 | 8.5525 | 0.1666 |
| **During 2.0 h** | | | | | | | |
| **Element** | **AN** | **Series** | **Net** | **(wt.%)** | **(Norm. wt.%)** | **(Norm. at.%)** | **Error in wt.% (1 Segma)** |
| Platinum | 78 | M-series | 11324 | 45.2450 | 45.2450 | 19.7562 | 1.3921 |
| Nickel | 28 | K-series | 3102 | 43.6560 | 43.6560 | 63.3576 | 1.1168 |
| Cobalt | 27 | K-series | 594 | 6.7227 | 6.7227 | 9.7169 | 0.1933 |
| Chromium | 24 | K-series | 729 | 4.3763 | 4.3763 | 7.1693 | 0.1353 |
| **During 2.5 h** | | | | | | | |
| **Element** | **AN** | **Series** | **Net** | **(wt.%)** | **(Norm. wt.%)** | **(Norm. at. %)** | **Error in wt.% (1 Segma)** |
| Platinum | 78 | M-series | 12,125 | 81.8981 | 81.8981 | 57.3841 | 2.4156 |
| Nickel | 28 | K-series | 662 | 16.5706 | 16.5706 | 38.5903 | 0.4400 |
| Chromium | 24 | K-series | 138 | 1.5313 | 1.5313 | 4.0256 | 0.0641 |

## References


1. Dec, J.; Sjoberg, M. *A Parametric Study of HCCI Combustion-The Sources of Emissions at Low Loads and the Effects of GDI Fuel Injection*; 2003-01-0752; SAE: Sydney, Australia, 2003.
2. Dec, J.; Sjoberg, M.; Hwang, W.; Davisson, M.; Leif, R.N. Detailed HCCI exhaust € speciation and the sources of hydrocarbon and oxygenated hydrocarbon emissions. *SAE Int. J. Fuels Lubr.* **2009**, *1*, 50–67. [CrossRef]
3. Kaiser, E.W.; Siegl, O.; Cotton, D.F.; Anderson, R.W. Effect of fuel structure on emission from a spark-ignited engine. 2. Naphthene and aromatic fuels. *Environ. Sci. Technol.* **1992**, *26*, 1581e1586. [CrossRef]
4. Kaiser, E.W.; Maricq, M.; Xu, N.; Yang, J. *Detailed Hydrocarbon Species and Particulate Emissions from a HCCI Engine as a Function of Air Fuel Ratio*; 2005-01-3749; SAE: Sydney, Australia, 2005.
5. Hasan, A.O.; Osman, A.I.; Al-Muhtaseb, A.H.; Al-Rawashdeh, H.; Abu-Jrai, A.; Ahmad, R.; Gomaa, M.R.; Deka, T.J.; Rooney, D.W. An experimental study of engine characteristics and tailpipe emissions from modern DI diesel engine fuelled with methanol/diesel blends. *Fuel Process. Technol.* **2021**, *220*, 106901. [CrossRef]
6. Mustafa, R.J.; Al-Rawashdeh, H.A.; Hassan, A.O.; Gomaa, M.R. Enhancement of a Hydrogen Engine Cavitation Utilizing Mixed Fuel: A Review and Experimental Case Study. *Int. Rev. Mech. Eng. (I.RE.M.E.)* **2020**, *14*, 33. [CrossRef]
7. Alahmer, A.; Rezk, H.; Aladayleh, W.; Mostafa, A.O.; Abu-Zaid, M.; Alahmer, H.; Gomaa, M.R.; Alhussan, A.A.; Ghoniem, R.M. Modeling and Optimization of a Compression Ignition Engine Fueled with Biodiesel Blends for Performance Improvement. *Mathematics* **2022**, *10*, 420. [CrossRef]
8. Sjöberg, M.; Dec, J.E. *EGR and Intake Boost for Managing HCCI Low-Temperature Heat Release over Wide Range of Engine Speed*; 2007-01-0051; SAE: Sydney, Australia, 2007.
9. Borges, M.E.; Díaz, L. Recent developments on heterogeneous catalysts for biodiesel production by oil esterification and trans esterification reactions: A review. *Renew. Sustain. Energy Rev.* **2012**, *16*, 2839–2849. [CrossRef]
10. da Costa Evangelista, J.P.; Gondim, A.D.; Souza, L.D.; Araujo, A.S. Alumina-supported potassium compounds as heterogeneous catalysts for biodiesel production: A review. *Renew. Sustain. Energy Rev.* **2016**, *59*, 887–894. [CrossRef]
11. Marinković, D.M.; Stanković, M.V.; Veličković, A.V.; Avramović, J.M.; Miladinović, M.R.; Stamenković, O.O.; Veljković, V.B.; Jovanović, D.M. Calcium oxide as a promising heterogeneous catalyst for biodiesel production: Current state and perspectives. *Renew. Sustain. Energy Rev.* **2016**, *56*, 1387–1408. [CrossRef]
12. Anwar, A.; Garforth, A. Challenges and opportunities of enhancing cold flow properties of biodiesel via heterogeneous catalysis. *Fuel* **2016**, *173*, 189–208. [CrossRef]
13. Schaberg, P.; Botha, J.; Schnell, M.; Hermann, H.; Pelz, N.; Maly, R. *Emissions Performance of GTL Diesel Fuel and Blends with Optimized Engine Calibrations*; Paper No. 2005-01-2187; SAE: Sydney, Australia, 2005.
14. Valencia, M.; López, E.; Andrade, S.; Iris, M.; Pérez, V.R.; de Lecea, C.S.M.; López, A.B. Proof of concept of the SCR of NOx in a real diesel engine exhaust using commercial diesel fuel and a full size Pt/beta zeolite/honeycomb monolith. *Catal. Commun.* **2014**, *46*, 86–89. [CrossRef]

15. Roy, S.; Hegde, M.; Madras, G. Catalysis for NOx abatement. *Appl. Energy* **2009**, *86*, 2283–2297. [CrossRef]
16. Liu, S.; Li, H.; Liew, C.; Gatts, T.; Wayne, S.; Shade, B.; Clark, N. An experimental investigation of $NO_2$ emission characteristics of a heavy-duty H2-diesel dual fuel engine. *Int. J. Hydrogen Energy* **2011**, *36*, 12015–12024. [CrossRef]
17. Abagnale, C.; Cameretti, M.; Simio, L.; Gambino, M.; Iannaccone, S.; Tuccillo, R. Numerical simulation and experimental test of dual fuel operated diesel engines. *Appl. Therm. Eng.* **2014**, *65*, 403–417. [CrossRef]
18. Hasan, A.O.; Al-Rawashdeh, H.; Abu-jrai, A.; Gomaa, M.R.; Jamil, F. Impact of variable compression ratios on engine performance and unregulated HC emitted from a research single cylinder engine fueled with commercial gasoline. *Int. J. Hydrogen Energy* 2022; *in press*. [CrossRef]
19. Lounici, M.S.; Loubar, K.; Tarabet, L.; Balistrou, M.; Niculescu, D.C.; Tazerout, M. Towards improvement of natural gas-diesel dual fuel mode: An experimental investigation on performance and exhaust emissions. *Energy* **2014**, *64*, 200–211. [CrossRef]
20. Yang, B.; Xi, C.; Wei, X.; Zeng, K.; Lai, M.C. Parametric investigation of natural gas port injection and diesel pilot injection on the combustion and emissions of a turbocharged common rail dual-fuel engine at low load. *Appl. Energy* **2015**, *143*, 130–137. [CrossRef]
21. Gomaa, M.R.; Mustafa, R.J.; Al-Dmour, N. Solar Thermochemical Conversion of Carbonaceous Materials into Syngas by Co-Gasification. *J. Clean. Prod.* **2020**, *248*, 119185. [CrossRef]
22. Tsolakis, A.; Golunski, S. Sensitivity of process efficiency to reaction routes in exhaust-gas reforming of diesel fuel. *Chem. Eng. J.* **2006**, *117*, 131–136. [CrossRef]
23. Cheenkachorna, K.; Poompipatpong, C.; Gyeung, C. Performance and emissions of a heavy-duty diesel engine fuelled with diesel and LNG (liquid natural gas). *Energy* **2013**, *53*, 52–57. [CrossRef]
24. Mohamed, A.; Nasser, W.S.; Kamel, B.M.; Hashem, T. Photodegradation of phenol using composite nanofibers under visible light irradiation. *Eur. Polym. J.* **2019**, *113*, 192–196. [CrossRef]
25. Khalil, A.; Aboamera, N.M.; Nasser, W.S.; Mahmoud, W.H.; Mohamed, G.G. Mohamed. Photodegradation of organic dyes by PAN/$SiO_2$-$TiO_2$-$NH_2$ nanofiber membrane under visible light. *Sep. Purif. Technol.* **2019**, *224*, 509–514. [CrossRef]
26. Abdelsayed, V.; Gardner, T.H.; Kababji, A.H.; Fan, Y. Catalytic conversion of $CO_2$ to propylene carbonate over Pt-decorated Mgsubstituted metal organic framework. *Appl. Catal. A Gen.* **2019**, *586*, 117225. [CrossRef]
27. Abu-Jrai, A.M.; Jamil, F.; Al-Muhtaseb, A.H.; Baawain, M.; Al-Haj, L.; Al-Hinai, M.; Al-Abri, M.; Rafiq, S. Valorization of waste Date pits biomass for biodiesel production in presence of green carbon catalyst. *Energy Convers. Manag.* **2017**, *135*, 236–243. [CrossRef]
28. Karre, A.V.; Kababji, A.; Kugler, E.L.; Dadyburjor, D.B. Effect of addition of zeolite to iron-based activated-carbon-supported catalyst for Fischer–Tropsch synthesis in separate beds and mixed beds. *Catal. Today* **2012**, *198*, 280–288. [CrossRef]
29. Saaed, W.; Elagawany, M.; Azab, M.M.; Amin, A.S.; Rath, N.P.; Hegazy, L.; Elgendy, B. Catalyst-and organic solvent-free synthesis, structural, and theoretical studies of 1-arylidenamino-2,4-disubstituted-2-imidazoline-5-ones. *Results Chem.* **2020**, *2*, 100042. [CrossRef]
30. Essa, K.; Sabouri, A.; Butt, H.; Basuny, F.H.; Ghazy, M.; El-Sayed, M.A. Laser additive manufacturing of 3D meshes for optical applications. *PLoS ONE* **2018**, *13*, e0192389. [CrossRef]
31. Hein, P.; Muller, L.; Körner, C.; Singer, R.F.; Muller, F.A. Cellular Ti–6Al–4V structures with interconnected macro porosity for bone implants fabricated by selective electron beam melting. *Acta Biomater.* **2008**, *4*, 1536–1544. [CrossRef]
32. Qiu, C.; Yue, S.; Adkins, N.J.E.; Ward, M.; Hassanin, H.; Lee, P.D.; Withers, P.J.; Attallah, M.M. Influence of processing conditions on strut structure and compressive properties of cellular lattice structures fabricated by selective laser melting. *Mater. Sci. Eng. A* **2015**, *628*, 188–197. [CrossRef]
33. Pourkhesalian, A.M.; Shamekhi, A.H.; Salimi, F. Alternative fuel and gasoline in an SI engine: A comparative study of performance and emissions characteristics. *Fuel* **2010**, *89*, 1056–1063. [CrossRef]
34. Gomaa, M.R.; Al-Dmour, N.; Al-Rawashdeh, H.A.; Shalby, M. Theoretical model of a fluidized bed solar reactor design with the aid of MCRT method and synthesis gas production. *Renew. Energy* **2020**, *148*, 91–102. [CrossRef]
35. Yusuf, A.A.; Yusuf, D.A.; Jie, Z.; Bello, T.Y.; Tambaya, M.; Abdullahi, B.; Muhammed-Dabo, I.A.; Yahuza, I.; Dandakouta, H. Influence of waste oil-biodiesel on toxic pollutants from marine engine coupled with emission reduction measures at various loads. *Atmospheric Pollut. Res.* **2022**, *13*, 101258. [CrossRef]
36. Okinaka, Y.; Wolowodiuk, C. Electroless Plating of Group Metls. *Electroless Plat. Fundam. Appl.* **1990**, *16*, 421–440.
37. Josso, P.; Alperine, S.; Steinmetz, P.; Costantini-Friant, A. *Hydrazinbath for Chemical Plating Platin and or Palladium and Process for Preparing Such a Bath*; EP 0423005 A1; Office National d'Etudes et de Recherches Aerospatiales (O.N.E.R.A.): Palaiseau, France, 1991.